Greenland tip jet and deep convection in the Irminger Sea: disentangling the roles of heat loss and wind stress

Aleksandr M. Fedorov[1,2], M. Femke De Jong[1], Claudia E. Wieners[2], Elodie Duyck[1], Henk A. Dijkstra[2]

[1]Royal Netherlands Institute for Sea Research (NIOZ), Department of Ocean Systems, Texel, the Netherlands
[2]Institute for Marine and Atmospheric research Utrecht (IMAU), Department of Physics, Utrecht University, Utrecht, the Netherlands

Correspondence to: Aleksandr M. Fedorov (aleksandr.fedorov@nioz.nl, amfedorov97@gmail.com)

Abstract. The strength of the Atlantic Meridional Overturning Circulation (AMOC) depends on deep-water formation in the Subpolar Gyre, particularly in the Irminger Sea, where convection is strongly modulated by short-lived but intense Greenland tip jet wind events. These mesoscale westerlies induce substantial surface heat loss and impose wind stress on the ocean, jointly influencing convective intensity. Using the high-resolution Parallel Ocean Program (POP) within the Community Earth System Model (CESM), we disentangle the thermal and mechanical effects of tip jet on mixed layer deepening through three ensemble experiments: full-forcing (heat loss + wind stress anomalies), heat-only, and wind-only, each compared to a climatological control run. All forced cases show a significant December–April deepening of the mixed layer relative to the control. The heat-only and full-forcing experiments produce similar mixed layer depth (MLD) increases (+1200 m; reaching ~1800 m), confirming that surface heat loss is the primary driver of deep convection. The wind-only case shows a smaller but still significant increase (+400 m; MLD ~1000 m), associated with enhanced early-winter mixing and wind-driven salinity increases in the upper ocean. This wind stress forcing erodes the fresh surface layer, reduces buoyancy, and promotes shear-driven mixing in December so that climatological winter heat loss can deepen the mixed layer more efficiently. Because wind stress is not projected to weaken under future warming, its mechanical influence may help delay or modulate the decline of convection in the Irminger Sea as surface heat loss decreases.

1 Introduction

Redistribution of heat across the Earth is partly accomplished by the ocean circulation. As a major component of the global conveyor belt, the Atlantic Meridional Overturning Circulation (AMOC) plays a key role in maintaining the mild climate of northern Europe (Jackson et al., 2015). In recent years, growing concern has emerged over the potential approach of an AMOC tipping point. Projections suggest that an irreversible weakening of the AMOC (e.g. van Westen et al., 2025) can occur in the near future. This weakening depends on a range of processes, among which the intensity of deep convection in the Subpolar Gyre is particularly critical (Desbruyères et al., 2019; Petit et al., 2020). The Irminger Sea, as part of the Subpolar Gyre, represents one of the main sites of deep convection that contributes to the strength of the AMOC (Nansen, 1906). In this region, episodes of intense surface heat loss drive enhanced winter convection (Pickart et al., 2003b; Våge et al., 2008).

One of the dominant atmospheric phenomena controlling heat loss in the Irminger Sea is the Greenland tip jet. The southern tip of Greenland is characterized by intense mesoscale wind events that form when synoptic-scale cyclones interact with Greenland's steep orography (Doyle and Shapiro, 1999; Moore, 2003; Pickart et al., 2003a). Blocked by Greenland's steep orography, the airflow is steered around the continental margin and accelerates near Cape Farewell, at Greenland's southernmost point. The two most frequent forms are the westerly, or direct, tip jet and the easterly, or reverse, tip jet (Outten et al., 2009; Renfrew et al., 2009b; Sproson et al., 2008; Våge et al., 2009a). Based on ERA-Interim reanalysis for 1990–2010, easterly tip jets occur during about 11% of the November–March period, while westerly tip jets occur during about 18% of this period (DuVivier et al., 2016). Although easterly tip jets are important for the western Irminger Sea and eastern Labrador Sea, including convection in the southeastern Labrador Sea (Sproson et al., 2008), the westerly tip jet produces the strongest negative buoyancy flux anomalies over the central Irminger Sea (DuVivier et al., 2016). Therefore, we focus here on the westerly tip jet, which drives convection intensity over the central Irminger Sea through large, localized heat loss and strong wind stress forcing(Moore and Renfrew, 2005). Although individual events last only a few days, their cumulative wintertime forcing can have a lasting influence on subpolar ocean convection and, ultimately, AMOC variability (de Jong and de Steur, 2016; Li et al., 2021; Lozier et al., 2019; Pickart et al., 2003b).

Tip jet influences ocean properties both thermodynamically and mechanically—through intense surface heat loss (Martin and Moore, 2007; Våge et al., 2008) and through momentum flux (Duyck et al., 2022). The heat loss component is known to directly trigger deep convection in the Irminger Sea (Josey et al., 2019). Observations and reanalyses confirmed that surface heat loss is the dominant factor in removing buoyancy from the Irminger Sea (Biló et al., 2022; de Jong et al., 2025). This buoyancy loss reduces stratification, deepens the mixed layer, and promotes dense water formation (de Jong et al., 2018; Våge et al., 2009b). In addition to surface heat loss, tip jets also exert a strong mechanical forcing on the ocean through momentum flux. The effect of this forcing on deep-water formation, however, remains much less explored. Observational and modeling studies show that variations in wind stress can drive changes in horizontal ocean transport (Fu et al., 2023; Sproson et al., 2010), including Ekman-driven freshwater export from the Greenland shelf near Cape Farewell (Coquereau et al., 2024; Duyck et al., 2022; Duyck and De Jong, 2021). This process is important for shelf–basin exchange and near-boundary stratification,

but ocean reanalysis and ocean modelling lagrangian studies suggest that the exported freshwater remains largely constrained by the boundary-current system, limiting its persistent direct influence on the main Irminger Sea convection region (Coquereau et al., 2024; Duyck et al., 2022). Here, we focus instead on the response of the interior upper ocean to tip jet wind-stress forcing, where enhanced shear and turbulent mixing can erode surface stratification and modify mixed-layer properties (Pollard et al., 1973; Price et al., 1986; Zhou et al., 2018); the extent to which this open-ocean pathway affects deep convection in the Irminger Sea remains poorly understood. Understanding this mechanism is particularly important in a warming climate, where surface heat loss is projected to weaken (Grist et al., 2023), while the mechanical forcing associated with westerly tip jet is expected to persist (Fedorov et al., 2025).

Here, we aim to disentangle the respective roles of enhanced heat loss and wind stress during Greenland tip jets in driving deep convection in the Irminger Sea using a high-resolution (0.1°) global ocean model. The Data and Methods section describes the model configuration, experiment design, and diagnostics used to quantify buoyancy content and ocean turbulence intensity. In the Results, we first examine the mixed layer depth (MLD) response in the Irminger Sea to tip jet heat loss anomalies, wind stress anomalies, and their combined forcing. We then analyze the corresponding salinity response across the same three experiments. Finally, we investigate the mechanisms by which wind stress modifies Irminger Sea convection. The last section summarizes our findings and places them in a broader context.

2 Data and Methods

2.1. Tip jet forced experiments and model setup

This study uses high-resolution ocean model output from the Parallel Ocean Program (POP v.2). We analyze daily and monthly fields of ocean properties (temperature, salinity, and velocity) on a curvilinear ~0.1° × 0.1° grid (≈6 × 11 km near Cape Farewell). The atmospheric forcing resolution is 0.25x0.25°, consistent with resolution requirements for robust assessments of tip jets (DuVivier and Cassano, 2013; Renfrew et al., 2009a; Shkolnik and Efimov, 2013; Sproson et al., 2010; Tilinina et al., 2014).

Using POP, we conduct four sets of ocean model simulations with different combinations of atmospheric forcing (see Fig.1d for the experimental design):

- **Control:** forced with the repeat annual climatological cycle only (CORE I normal-year forcing, more detail follows below).
- **Full-forcing**: climatological cycle plus tip jet anomalies in heat loss and wind stress.
- **Wind-only**: climatological cycle plus the tip jet wind stress anomaly only.
- **Heat-only**: climatological cycle plus the tip jet heat loss anomaly only.

The control run is forced with the repeat annual atmospheric climatological cycle ("normal-year") from the Coordinated Ocean-ice Reference Experiments (Large and Yeager, 2004) (CORE I, [https://www.clivar.org/clivar-panels/omdp/core-1]).

The model spin-up lasted 300 years (years 1–299 are treated as spin-up), after which temperature and salinity drift remained within stable bounds. The total length of the control dataset used for the reference ocean climatology is 24 years (years 300–323), which we treat as the quasi-equilibrated control segment for analysis. For comparison with the tip jet experiments, we compute a 1-year daily and monthly climatology from these 24 years and repeat it six times to form a continuous 6-year reference. For the daily climatology, the repeated cycle is smoothed with a 14-day moving mean to ensure seamless transitions between December and January. Additional details on the high-resolution POP model configuration used here are provided in Viebahn et al. (2016).

The three tip jet experiments are forced with composite anomalies of surface heat loss and wind stress derived from ERA5 reanalysis on tip jet days for 1969–2022. In the ERA5 data, tip jet days are identified when wind speed is within the strongest 10% and the flow direction is westerly (Duyck et al., 2022; Moore, 2012). In the next step, we compute composite mean anomalies of net surface heat flux and wind stress relative to the 1969–2022 long-term mean for the identified tip jet days in the ERA5 period. In this study, heat loss refers to negative values of net surface heat flux, corresponding to a heat flux directed out of the ocean. The net surface heat flux includes turbulent sensible and latent heat fluxes, as well as longwave and shortwave radiative fluxes, as derived from ERA5. These composites of wind stress and heat loss anomalies (Fig. 1a,b; see Fedorov et al., 2025 for details) are then added to the CORE forcing within the area outlined by the red contour in Fig. 1a,b to create the forcing fields.

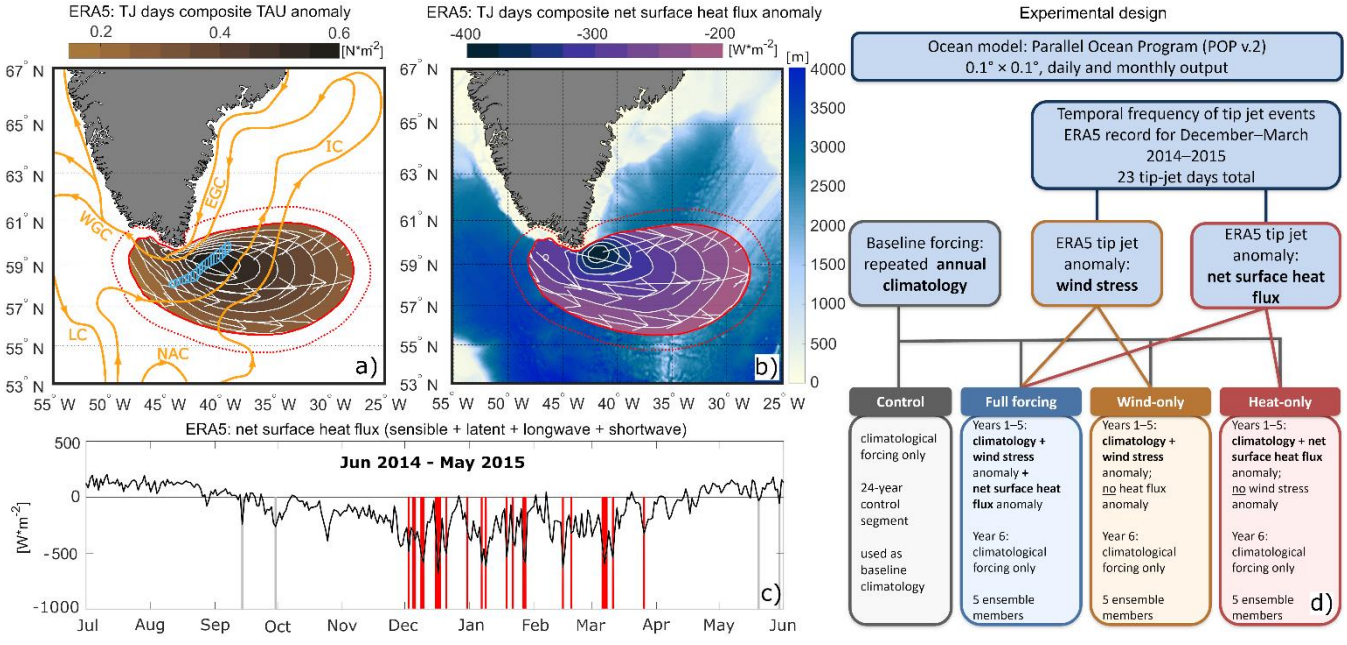

Figure 1. Study domain, composite tip jet (TJ) forcing fields, and definition of analysis region. (a) ERA5 composite of wind stress (TAU) anomalies on tip jet days (relative to the 1969–2022 climatology; Fedorov et al., 2025). The red outline marks the region where

wind stress anomalies were added to the CORE I model forcing. The red dotted outline indicates the tapering zone, where the imposed anomaly gradually decreases to zero. Cyan shading indicates the convective area (March mean MLD > 1000 m in the full-forcing experiment). Orange contours show the mean DJFM surface circulation (0–100 m). Currents: IC – Irminger Current, EGC – East Greenland Current, WGC – West Greenland Current, LC – Labrador Current, NAC – North Atlantic Current. White arrows show the wind direction. (b) ERA5 composite of net surface heat-flux anomalies for the same tip jet days. White arrows show the wind direction. Background colour shows ETOPO 2022 bathymetry [https://doi.org/10.25921/fd45-gt74]. (c) Daily net surface heat flux averaged over the forcing region for 2014–2015. The black curve shows total flux, while vertical bars indicate days with tip jet conditions during DJFM (red) and in other months (grey). Negative values indicate heat loss from the ocean. (d) Schematic of the experimental design.

The forcing region and forcing frequency were determined in a separate case study (Fedorov et al., 2025). The forcing area (Fig. 1a,b) corresponds to the zone enclosed by approximately the 50% contour of the peak wind stress anomaly and is chosen to confine the effect of tip jet to the interior of the Irminger Basin. To prevent strong gradients at the forcing boundary, the anomaly amplitudes taper smoothly to zero across a 10-grid-cell (~100 km) buffer. This tapering does not remove wind-stress gradients entirely, but smooths over a broader area. We checked whether the mixed-layer-depth shows consistent signal (in line with Ekman upwelling or downwelling) along the edge of the forcing mask and found no boundary-following MLD signal; instead, the strongest deepening occurs in the interior Irminger Basin, where the imposed forcing is largest and where the convective region is defined. To prescribe the temporal frequency of tip jet events, we use the ERA5 record for December–March 2014–2015, which represents the strongest tip jet winter on record for 1969–2022 (Fig. 1c; Fedorov et al., 2025). 23 tip jet days were identified from December 2014 to March 2015 (Fig. 1c), compared to a long-term winter mean of 11±6 tip jet days per cold season. We use the strongest tip jet winter on record to robustly disentangle the effect of tip jets from background climate variability.

Each forced case is run as a five-member ensemble. Each ensemble member spans six years (Fig. 1d): the first five years include tip jet forcing applied on all DJFM days on which tip jets occurred in 2014–2015, while the sixth year reverts to the standard CORE forcing. The sixth year allows us to assess how long the model response persists after the tip jet anomalies are removed and the forcing returns to the repeat annual climatological cycle. Each member is initialized from a different year of the control run, with start years spaced five years apart, to sample different NAO phases and to reduce the likelihood that ensemble members share the same model internal variability. We then compute the ensemble mean, yielding a six-year time series that is compared to the control run throughout the analysis. The same ensemble design is applied to all three tip jet forced experiments (full forcing, wind-only, and heat-only).

When comparing the forced runs with the control, we assessed statistical significance using a random permutation (randomization) test applied to the replicated samples available for each calendar time step (e.g., Good, 2005). For each quantity and each calendar day (or month), we computed the observed difference ($\Delta_{\mathrm{obs}} = \bar{X}_{\mathrm{forced}} - \bar{X}_{\mathrm{control}}$), where $\bar{X}$ denotes the mean across realizations. The null hypothesis is that the forced and control realizations have equal means ($H_0: \mu_{\mathrm{forced}} = \mu_{\mathrm{control}}$). The forced experiment provides 25 realizations (five ensemble members × five years), while the control provides 24 realizations (years 300–323). To generate the null distribution, we pooled the 49 realizations and randomly reassigned them into two groups of the same sizes as the original samples, 25 and 24. Under this random reassignment, the

group labels no longer correspond to the original experiment labels, so each permuted group can contain a mixture of originally forced and control realizations. For each permutation, we recomputed the difference between the two group means, repeating this procedure 2000 times. A difference is considered significant at the 95% level if Δ_{obs} lies below the 2.5th percentile or above the 97.5th percentile of this null distribution (two-sided test; $p < 0.05$). We used the same approach when comparing the tip jet experiments to each other. Throughout the paper, whenever we state that a difference is "significant", we refer to significance at the 95% level according to this permutation test. This procedure is closely related to a (block) bootstrap test of the difference in means, but constructs the null distribution by random reassignment of labels rather than resampling with replacement.

2.2. Surface Buoyancy flux and Ocean Buoyancy content

Using the four modeled datasets, we quantify the impact of tip jets on stratification by estimating the buoyancy content of the water column (B_{ocean}, Eq. 1) and the surface buoyancy flux (B_{flux}, Eq. 2). Following Schmidt and Send (2007), identical assessments of B_{ocean} were previously applied to the Irminger Sea (Biló et al., 2022; de Jong et al., 2025). We adopt the same approach here:

$$B_{ocean} = \frac{g}{\rho_0}\int_0^D \left(\sigma_0(z) - \sigma_0(z_0)\right)dz;\ [m^2\ s^{-2}]\,, \tag{1}$$

where D is a specific vertical depth (positive downward), g = 9.8 m s^{-2} is gravitational acceleration, ρ_0 = 1027 kg m^{-3} is the reference density, $\sigma_0(z)$ is the potential density at depth z, and $\sigma_0(z_0 = 0)$ is the potential density at the surface.

We compute B_{flux} as the buoyancy flux associated with net surface heat fluxes (Gill, 1982):

$$B_{flux} = \frac{g}{\rho_0}\frac{\alpha}{C_p}\,Q_{net};\ [m^2\ s^{-3}]\,, \tag{2}$$

where, α is the thermal expansion coefficient (which itself is a function of temperature and salinity), C_p is the specific heat capacity of seawater at constant pressure, Q_{net} is the net surface heat flux.

We do not include the haline (freshwater) component ($\beta g S_0(E - P)$) of the buoyancy flux, because tip jets have no significant impact on precipitation in this region (DuVivier et al., 2016), and we do not include an evaporation–precipitation anomaly forcing in our experiments. We derive density and all thermodynamic parameters using the Gibbs-Sea Water (GSW) relation (McDougall and Barker, 2011)[https://www.teos-10.org/software.htm]). Both B_{ocean} and B_{flux} are spatially averaged over the region where the mean March MLD exceeds 1000 m in the full-forcing ensemble (Fig. 1a, cyan-shaded area), hereafter referred to as the convection region. We define this region from the full-forcing experiment because it includes both wind stress and heat loss anomalies and therefore provides the most realistic representation of tip jet-driven convection. This fixed region is then applied consistently across all experiments to facilitate a direct comparison of their responses.

2.3. Shear and Richardson number

To assess the potential for wind-driven mixing during tip jet events, we diagnose vertical shear (Eq. 3), buoyancy frequency (Eq. 4) and the gradient Richardson number (Eq. 5) from the model velocity and density profiles in the convective region.

The squared vertical shear of horizontal velocity is defined as:

$$S^2 = \left(\frac{\partial u}{\partial z}\right)^2 + \left(\frac{\partial v}{\partial z}\right)^2, [s^{-2}], \quad (3)$$

where u and v are the zonal and meridional velocities.

The buoyancy frequency is defined as

$$N^2 = -\frac{g}{\rho_0}\frac{\partial \rho}{\partial z}, [s^{-2}], \quad (4)$$

where ρ is the modelled in-situ density.

The gradient Richardson number is then given by

$$Ri = \frac{N^2}{S^2}, \quad (5)$$

We compute S^2, N^2, and consequently Ri in each model layer, starting from the surface. For the daily time-series analysis, we spatially average these quantities over the convection region (Fig. 1a), yielding a daily mean vertical profile. We then average these daily profiles across all ensemble members for each case. The resulting 5-year daily time series (tip jet-forced years only) is further averaged by day-of-year to obtain the mean annual cycle of S^2 and Ri. We perform this daily time-series analysis only for the wind-only experiment. We additionally verified that no comparable response occurs in the heat-only experiment by comparing daily surface fields of Ri and S^2 between the heat-only and wind-only runs.

According to the Miles–Howard criterion (Howard, 1961; Miles, 1961), flows with a gradient Richardson number $Ri < 0.25$ are susceptible to shear-driven instability. Similar thresholds are widely used in upper-ocean mixing studies (Large and Crawford, 1995; Monin and Obukhov, 1954; Pollard et al., 1973; Price et al., 1986). POP employs the same stability logic internally through the K-Profile Parameterization (KPP; (Large et al., 1994)), which computes shear and stratification at every baroclinic timestep (~1 h). When $Ri < 0.25$, KPP increases the vertical mixing coefficients for momentum and tracers and, when the instability occurs near the mixed layer base, entrains water upward into the mixed layer. Because POP outputs daily-mean velocity and density fields, the diagnosed Ri is a time-averaged quantity that is systematically higher than the instantaneous Ri used by KPP. Therefore, the Ri computed from our model output should be interpreted as a qualitative indicator of the relative susceptibility to shear-driven mixing, not as a direct measure of instability events (Large et al., 1994).

3 Results

3.1. Tip Jet heat loss as a primary driver of convection

3.1.1. Mixed layer depth response

Our model results highlight the dominant role of surface heat loss during tip jets in driving deep convection. All simulations show a winter increase in mixed layer depth (MLD) in the central Irminger Sea. In the control run, MLD reaches about 400 m in February, deepens further to 600-700 m and expands horizontally in March (Fig. 2, row 4). Relative to the control, the full-forcing run shows a sharp and statistically significant (95 %) deepening of MLD during JFMA (Fig. 2, row 1). A magnitude and spatial extent of deepening similar to the full-forcing run occurs in the heat-only run (Fig. 2, row 3). In both the full and heat-only experiments, MLDs increase basin-wide by 400–800 m in February–March compared to control, approaching observed maxima of ~1400 m in the region (Fedorov et al., 2023; Fedorov and Bashmachnikov, 2020; de Jong et al., 2025; de Jong and de Steur, 2016). By contrast, the wind-only run (Fig. 2, row 2) produces weaker deepening of up to ~400 m relative to the control. However, MLD maxima of ~1000 m are still reached in March in a smaller region, despite the absence of enhanced surface heat loss forcing. These results indicate that heat and wind surface fluxes can each enhance convection separately.

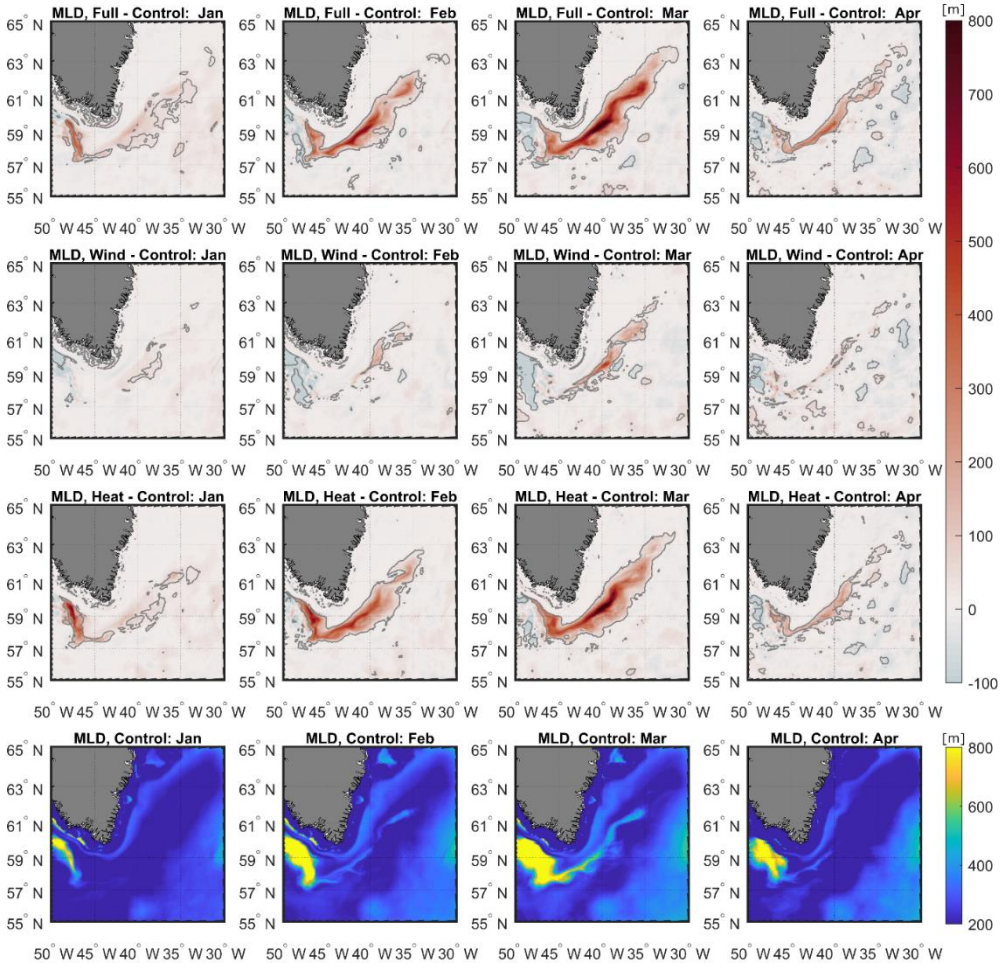

Figure 2. Monthly mixed layer depth (MLD) differences relative to the control run in the Irminger Sea. Columns represent January–April (left to right). Rows show: (top) full-forcing minus control, (second) wind-only minus control, (third) heat-only minus control, and (bottom) the corresponding monthly mean MLD from the control run. Grey contours indicate regions where MLD differences are significant at the 95 % confidence level.

The temporal evolution of the MLD also differs. Within the region of deepest convection (>1000 m in the full-forcing in March; Fig. 1a, cyan shading), winter mean MLD is generally greater in the full-forcing run than in the heat-only run, but both remain in the 1100–1300 m range each year, with maxima up to 1800 m (Fig. 3a). The wind-only run shows shallower convection (800–900 m on average, maxima ~1300 m), but still deeper than the control (600 m mean, ~1000 m maximum). Across the five-year ensembles, MLD gradually becomes shallower in all experiments, with the largest decline in the wind-only run, which approaches control values by year 5. Although the sixth year is forced climatologically the enhanced MLDs remain in the heat-only run, while mean and maximum MLDs in the full-forcing and wind-only runs are very close to the control. Therefore, enhanced heat loss has a more persistent effect on MLD in the Irminger Sea than wind stress alone.

3.1.2. Buoyancy flux and ocean buoyancy content

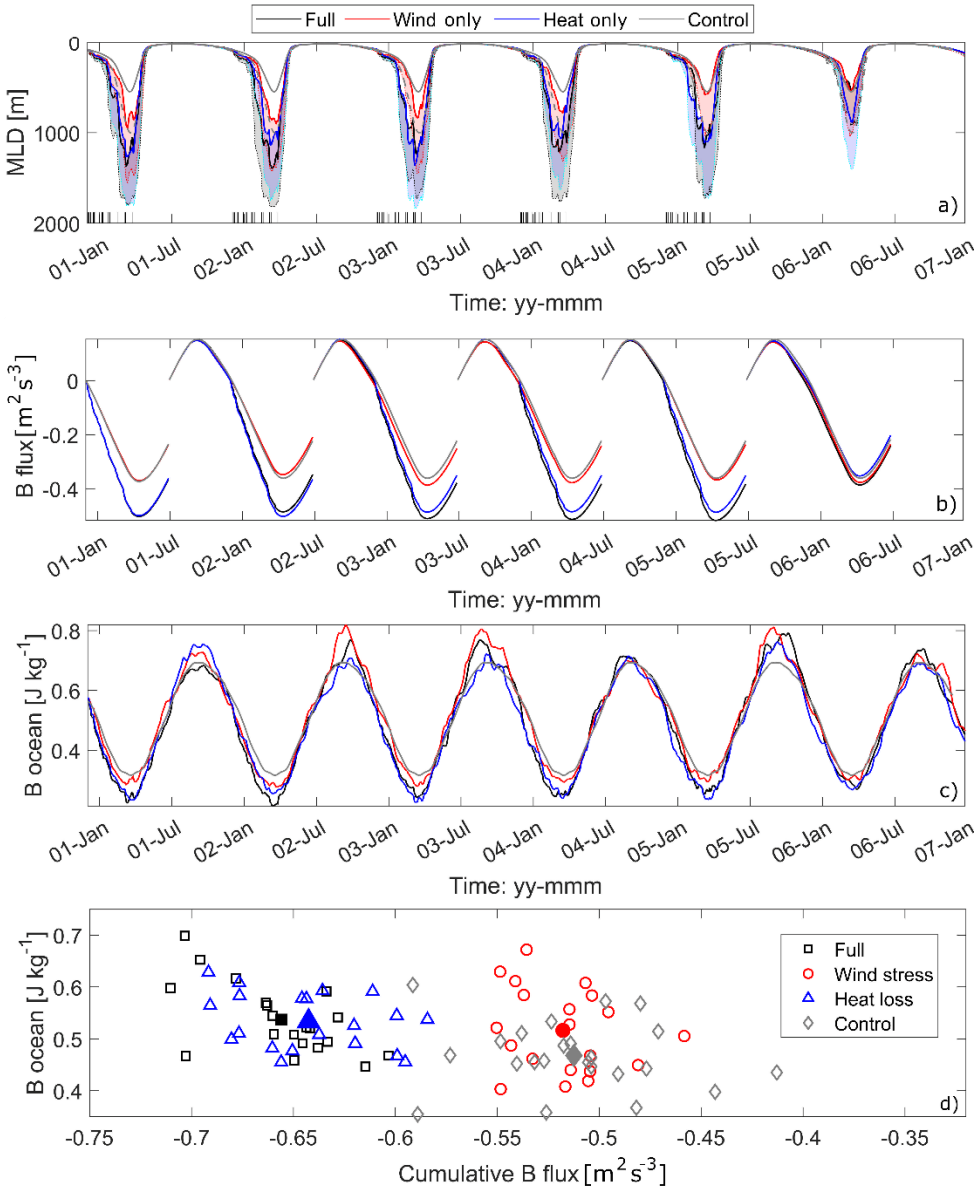

Figure 3. Temporal variability in the convective region (Fig. 1a) for ensemble means. Colours: black = full-forcing, red = wind-only, blue = heat-only, grey = control. (a) Mixed-layer depth (MLD). Shading indicates +1 standard deviation (toward deeper values): light grey with dotted black outline (full-forcing), light red with dotted red outline (wind-only), and light blue with dotted blue outline (heat-only). The grey dashed line marks the upper bound of control variability. Black vertical bars at the bottom of the panel show periods when tip jet forcing was applied. (b) Cumulative surface buoyancy flux (B_{flux}) (integrated from July 1 of the previous year to July 31 of the following year). (c) Ocean buoyancy content (B_{ocean}). (d) Scatter plot of seasonal B_{ocean} change (year maximum in September – minimum in the following March) versus cumulative B_{flux} at end-April, for years 02–05 (20 years per experiment). Filled markers indicate multi-year means.

The effects of tip jet heat loss can be interpreted from the buoyancy forcing in the central Irminger Sea. In our experimental setup we apply heat loss anomalies in the full-forcing and heat-only runs, whereas the wind-only experiment retains climatological heat loss. The cumulative buoyancy flux (B_{flux}), integrated from 1 July to 30 June each year (Fig. 3b), is nearly identical in the full-forcing and heat-only runs. In contrast, B_{flux} in the wind-only run remains within the range of the control simulation, consistent with the absence of a heat loss anomaly.

The response to surface buoyancy flux is reflected in differences in ocean buoyancy content (B_{ocean}) among the runs (Fig. 3c). B_{ocean} is generally highest at the end of summer, during which buoyancy input exceeds buoyancy loss, and decreases during the cooling season (September–March) as the buoyancy removal rate increases with surface fluxes. This seasonal decrease also occurs in the wind-only experiment because this case still includes the climatological net surface heat flux. Thus, the wintertime decrease in B_{ocean} in the wind-only case does not require an imposed tip jet heat-flux anomaly. The evolution of B_{ocean} is broadly consistent with the surface buoyancy flux and MLD: the full-forcing and heat-only runs show nearly identical lowest March values, while the wind-only run remains between them and the control, which shows the highest winter B_{ocean}. In summer, B_{ocean} in the wind-only run is either the highest among all experiments (years 02, 03, and 05) or comparable to the other runs. However, the decrease in B_{ocean} from September to March is nearly the same as in the heat-only and full-forcing runs. The key point is that this enhanced seasonal decrease occurs relative to the control without an additional heat-flux anomaly: the cumulative B_{flux} in the wind-only case remains within the range of the control simulation (Fig. 3b,d). Relative to the control, the buoyancy-removal rate in the wind-only run is higher by ~25–30% (0.51–0.53 $J\ kg^{-1}\ yr^{-1}$ versus 0.38 $J\ kg^{-1}$ yr^{-1}), even though no additional heat loss forcing is applied in this experiment. This indicates that wind stress modifies the ocean buoyancy response through processes not captured by the cumulative surface buoyancy flux alone.

Further, we compare the annual B_{ocean} change and the cumulative surface buoyancy flux (B_{flux}) (Fig. 3d). The simulations with heat-only forcing differ significantly (95 % confidence) from those without heat-flux anomalies, and this difference comes directly from differences in B_{flux}. However, the B_{ocean} change in the wind-only run remains comparable to that in the full-forcing and heat-only runs rather than to control, even though its B_{flux} is much weaker. This separation between surface forcing and ocean buoyancy response indicates that, in the wind-only experiment, wind stress modifies the upper-ocean buoyancy evolution through processes not captured by the cumulative surface buoyancy flux alone. The following sections examine this wind-driven response in terms of salinity redistribution, shear, and mixing potential.

3.2. Irminger Sea response to tip jet wind stress forcing

3.2.1. Salinity response to tip jet forcing

Having established that heat loss is the primary, but not the only, driver of the deepest convection, we now examine how wind stress can modify upper-ocean properties in the Irminger Sea. We focus on the impact of Greenland tip jet wind stress on the basin interior. In our model experiments, Greenland tip jets not only enhance surface cooling but also increase surface salinity in the interior of the Irminger Sea (Figs. 4–5).

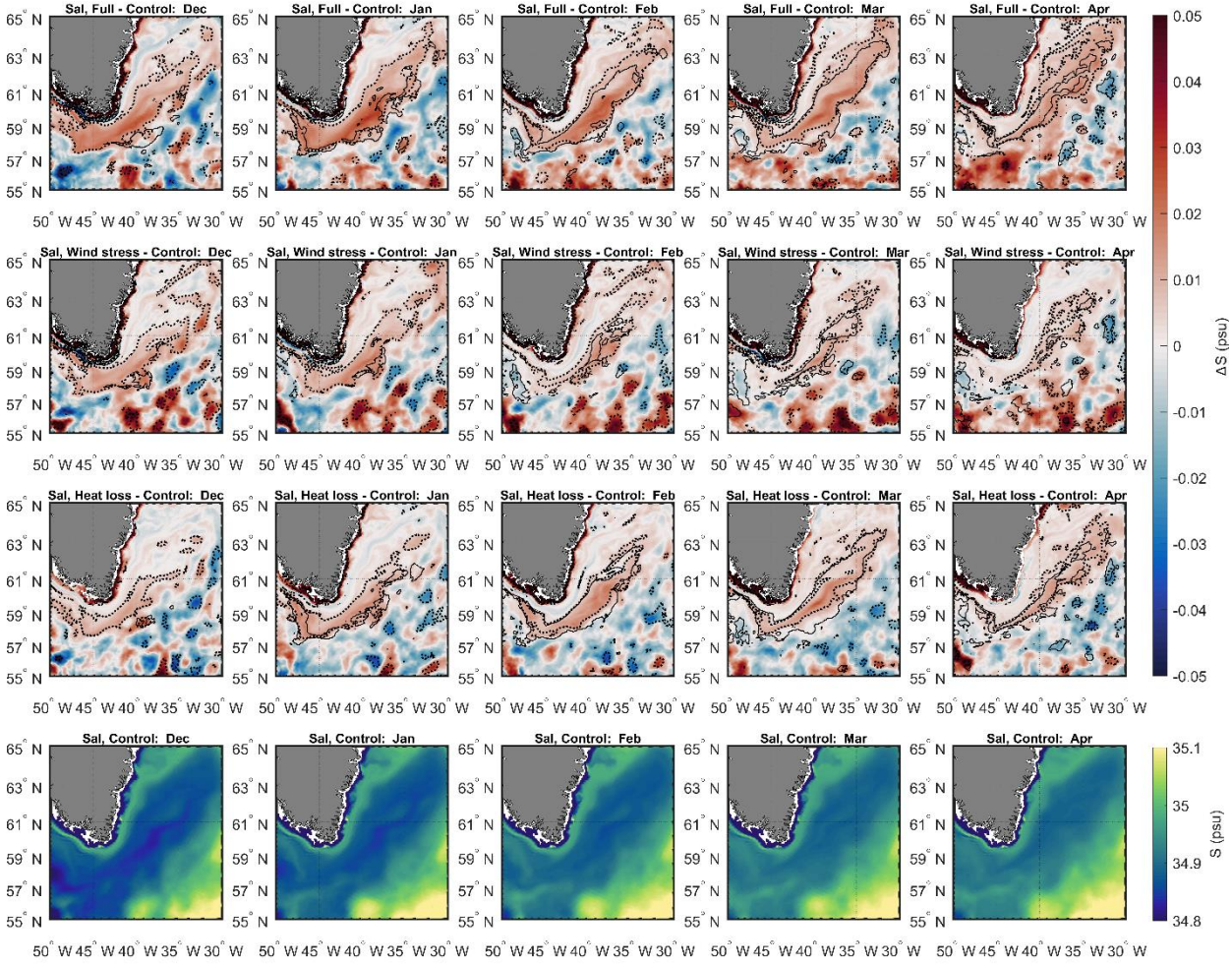

Figure 4 Monthly upper-ocean salinity anomalies relative to the control run in the Irminger Sea. Columns represent December–April (left to right). Rows show: (top) full-forcing minus control, (second) wind-only minus control, (third) heat-only minus control, and (bottom) the corresponding monthly mean salinity from the control run (upper 100 m). Black dotted contours indicate regions where salinity anomalies are significant at the 95 % confidence level, and black solid contours indicate regions where MLD differences are significant at the 95 % confidence level.

The upper 100 m is saltier in all forced runs than in the control (Fig. 4, rows 1–3). In the control (row 4), salinity is relatively low in the narrow coastal band around Greenland, increases across the East Greenland Current (EGC), and decreases toward the central Irminger Basin. Full tip jet forcing produces a positive salinity anomaly over large areas of the central Irminger Sea following the imposed forcing from December to March (Fig. 4, row 1). In the wind-only case (Fig. 4, row 2), a similar positive salinity anomaly dominates in December–January, but its spatial extent is significantly smaller than in the full-forcing case during February–April. The heat-only case also shows a positive salinity anomaly (Fig. 4, row 3); however, in December–January it covers the smallest area among the forced runs, while it expands in February–March and exceeds the wind-only run.

The seasonal evolution differs between the heat-only and wind-only experiments. In the heat-only case, salinity anomalies strengthen and expand as the mixed layer deepens: early in winter, when MLD is shallow, the anomaly is confined to regions where buoyancy loss triggers mixing, whereas it becomes strongest and most widespread in February–March as MLD approaches its maximum. The wind-only case shows the opposite timing: surface salinity increases primarily in December–January while MLD is still relatively shallow, consistent with the wind stress anomaly initiating the salinification. These contrasting behaviors are also reflected in the full-forcing run, where the salinity anomaly remains persistently high throughout December–April.

We see a similar salinity response on the spatially averaged vertical profile inside the convective region (Fig. 5). In the control run (Fig. 5d), the upper 250–300 m of the Irminger Sea interior is fresher than the waters below. This near-surface fresh layer is most pronounced during September–January, associated with summer ice melt around Greenland. During winter convection, it is mixed with the saltier subsurface waters. The presence of saltier subsurface waters enables a pronounced increase in salinity in the upper ~250 m when vertical mixing is strengthened by tip jet forcing (Fig. 5a–c). This surface salinity increase is accompanied by a comparable decrease in salinity in the layers just below, indicating vertical redistribution of salt within the interior water column. Thus, the salinification diagnosed in the convective region reflects local mixing and entrainment rather than a persistent lateral freshwater signal from the shelf.

We can conclude that the vertical penetration of the salinity anomaly depends on convection depth: the full-forcing and heat-only runs (with deeper MLD) exhibit salinity increase in deeper layers than the wind-only run. Consistent with this, salinity is significantly lower in the wind-only run than in the heat-only run (Fig. 5f) during mid-February to mid-April. Overall, tip jet forcing in all experiments increases surface salinity by bringing saltier subsurface water to the surface through intensified winter convection.

The growth of salinity in the heat-only run is primarily caused by the increase in surface heat loss during tip jet events. Surface heat loss reduces buoyancy in the upper layers and enhances deep convection to extreme depths of about 1800 m, bringing salinity upwards. At first sight, the full-forcing run has a similar salinity increase in the upper 250 m and comparable MLDs (Fig. 5a,c), which indicates that similar processes act to increase salinity there. However, when we compare the full-forcing run directly to the heat-only run (Fig. 5e, the full 5-year daily time series is available in the appendix Fig. A1), the upper-layer salinity in the full-forcing run is significantly (95 %) higher in December–March. Therefore, the reason for the differences between full-forcing and heat-only runs must come from the wind stress.

The role of wind stress can also be considered separately from the heat loss. While the MLD in the wind-only run is less than in the heat-only run, it is higher than in the control. This MLD increase is associated with the corresponding growth in surface salinity. During December in the wind-only run, salinity in the upper 70 m is not only higher than in the control run but also higher than in the heat-only run (Fig. 5f). This salinity increase has a clear mixing signature, being accompanied by lower salinity values below the mixed layer. This salinity anomaly is significant and traceable until the MLD in the heat-only run (dashed) outgrows the one in the wind-only run (solid) by the end of December. Thus, wind stress during tip jet events is capable of causing an intensification of mixing already in December.

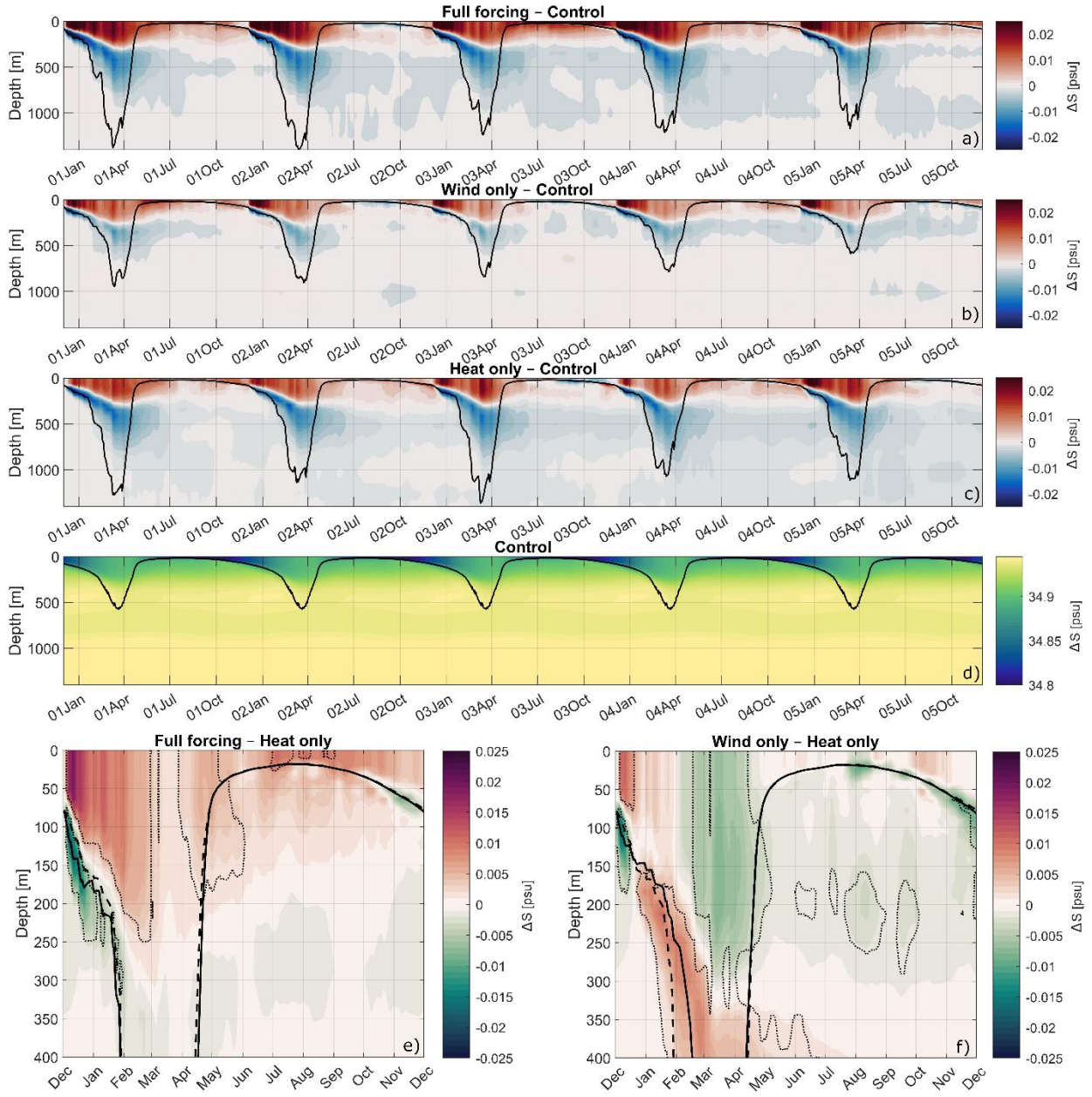

Figure 5. Response of salinity to tip jet forcing in the convective region. (a–d) Temporal evolution of area-averaged salinity anomalies (psu): (a) full-forcing – control, (b) wind-only – control, (c) heat-only – control, (d) control reference. Black curves show the MLD. Annual mean salinity differences: (e) full forcing – heat-only, (f) wind-only – heat-only. The black solid line shows annual mean MLD in the full forcing (e) or wind-only (f) and the dashed one shows the MLD for heat-only run. Thin dotted lines mark depths where salinity differences between the runs are significant at the 95 % confidence level.

3.2.2. Turbulent response of the ocean to wind stress forcing

We next examine the upper-ocean response to the wind stress perturbation in terms of shear and stratification. In the wind-only run, the imposed wind stress anomaly produces a distinct increase in vertical shear within the forcing region (relative to the control and heat-only runs), particularly between the surface layer (0 m) and the layer below (10 m) (Fig. 6a). This signal is absent in the heat-only simulation, because it lacks the additional wind stress forcing. The impact of the wind-driven shear anomaly on the surface layer can be qualitatively assessed using the gradient Richardson number (Ri), which reflects the balance between stratification and shear (Sect. 2.3). As mentioned there, POP provides daily-mean output and employs parameterized turbulence and the diagnosed Ri should be interpreted as a qualitative indicator rather than a direct measure of instantaneous instability. The classical Miles–Howard threshold of Ri < 0.25 applies to instantaneous shear instability, whereas our Ri values are computed from daily-mean fields. Daily averaging smooths short-lived low-Ri events and therefore shifts the Richardson number based stability diagnostic toward larger, more stable values. We therefore use Ri < 1, not as a strict instability threshold, but as an indicator of regions where the potential for shear-driven mixing remains elevated even after daily averaging. Even with these limitations, the daily fields show a clear reduction in Ri in the wind-only run (Fig. 6b), with values < 1 concentrated in the convection region during a representative December wind stress event. These Ri anomalies indicate increased susceptibility to shear-driven mixing in this area, consistent with the December MLD deepening and the consequent surface salinity increase in the wind-only run.

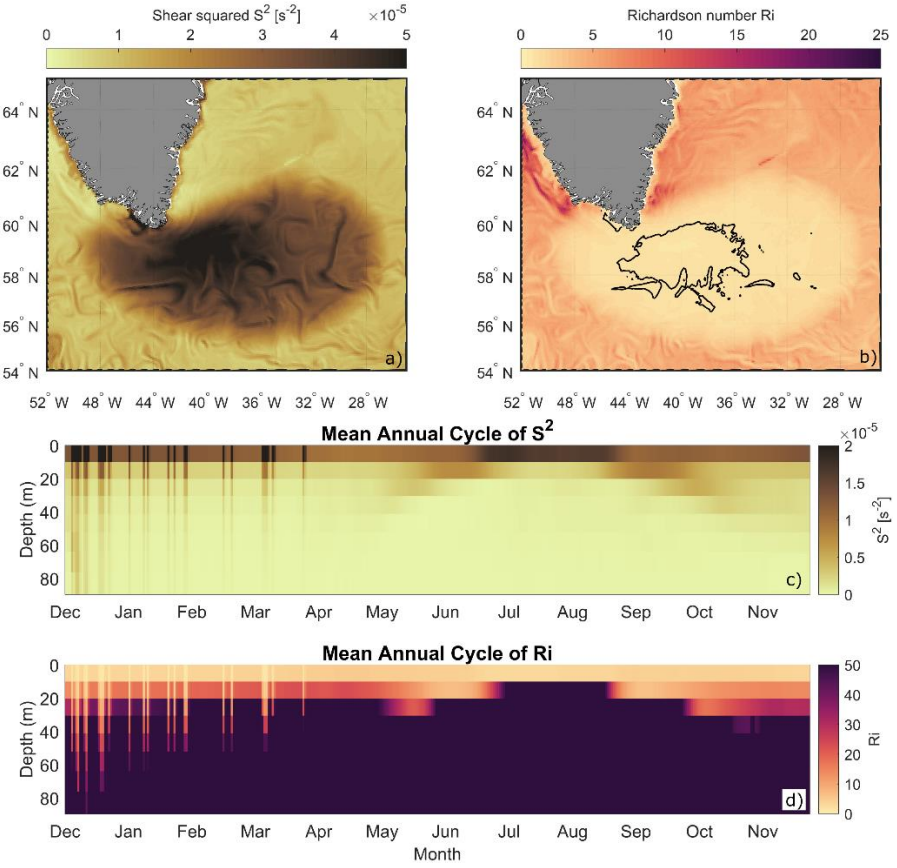

Figure 6. Shear and Richardson number in the wind-only run. A 1-day December wind event: (a) Shear squared over the surface and layer below (10 m), (b) Richardson number over the same layers. The black contour shows the area where the gradient Richardson number is less than 1. (c–d). Climatological ensemble mean profile timeseries in the upper 100 m in the convective region: (c) velocity shear squared, (d) gradient Richardson number.

Shear anomalies associated with the wind forcing are not restricted to the very surface; they propagate downward and remain detectable through the upper ~100 m (Fig. 6c). In the annual cycle, the signature of the wind stress perturbation appears during the tip jet days (December–March), when shear increases in the convective region. The largest shear differences occur in the upper 0–30 m and extend deepest during December (the annual maximum wind stress in CORE), with a progressively shallower response from January to March. This timing matches the MLD and salinity increase in the wind-only run (Fig. 5f), where erosion of the fresh surface layer is also strongest in December.

Together with the salinity anomalies in Fig. 4-5, this supports the interpretation that tip jet wind stress acts primarily as an early-winter trigger mechanism, giving the early shallow mixed layers an extra push and helping them erode the upper ocean salinity stratification, rather than a direct driver of the deepest mixed layers. This interpretation is consistent with Zhou et al. (2018), who used a different regional setting but similarly partitioned heat and momentum forcing and showed that wind forcing can deepen the mixed layer through mechanical effects. In December, enhanced shear promotes vertical mixing, which transports salinity upward and erodes the fresh surface layer. This reduces the buoyancy of the upper ocean. Once this initial

barrier is weakened, the climatological winter heat loss becomes more effective at deepening the mixed layer. As a result, convection can reach deeper layers later in the season compared to the control simulation.

4 Summary and Discussion

In this study we investigated the impact of Greenland tip jets on deep convection in the Irminger Sea using a high-resolution ocean model forced with composite tip jet anomalies of wind stress and heat loss. Our goal was to disentangle the relative roles of thermal and mechanical forcing and to assess how they influence buoyancy content, surface fluxes, convection and ocean properties in the interior of the Irminger Sea.

Our results confirm that surface heat loss during tip jets is the dominant driver of convection intensity. Both the full tip jet forcing (heat loss + wind stress) and the heat-only experiment produce mixed layer depths of similar magnitude (1100–1300 m mean and ~1800 m maximum versus 600 m in control). The close resemblance between the heat-only and full-forcing runs is consistent with the dominant role of surface heat loss in removing buoyancy from the water column and thus triggering deep convection in the Irminger Sea (Biló et al., 2022; de Jong et al., 2025).

In general, the response of the MLD to wind-only forcing is weaker, yet still statistically significant at the 95% level. However, in December the MLD response is comparable to the full-forcing run and exceeds the heat-only run. In other months, the wind-only experiment produces shallower mixed layers than the other forced runs but remains much deeper than the control (maximum in March: ~1000 m in wind stress run versus 600 m in control). As this experiment is forced solely with wind stress anomalies, its effect is mechanical: the imposed westerly winds increase vertical shear between the surface layer and the underlying water column. The enhanced shear and the associated low Richardson numbers indicate higher potential for shear instability and vertical turbulent mixing in early winter. This increased vertical mixing leads to increased salinity in the surface layer at the beginning of the tip jet forcing in December. The additional salinity removes buoyancy from the fresh upper layer early in winter and reduces the stabilizing influence of the Greenland meltwater on convection development during the rest of the cold season.

This effect of the wind stress on salinity is most significant at the beginning of the convective season in December, when the MLD is relatively shallow (confined to roughly the upper 100 m). Later in winter, the effect of wind stress weakens, but at this point the moderate (from climatology) heat loss is capable of deepening the MLD further than in the control because part of the buoyancy has already been removed at the start of winter by tip jet wind stress. In this sense, wind stress acts mainly as an early-winter MLD trigger mechanism that facilitates deeper convection later in the season, rather than as the primary driver of the deepest mixed layers.

Our analysis has several limitations related to model output, resolution, and experimental design. The coarse vertical resolution in the upper ocean and the use of daily-mean output constrain our ability to diagnose turbulent processes. POP computes shear, stratification, and Richardson numbers at every baroclinic timestep (~1 h), but the fields available for analysis represent 24-hour averages. Because Ri is highly nonlinear in shear, daily averaging smooths out short-lived shear instabilities,

systematically biasing the diagnosed Ri toward more stable values. Classical Ri based parameterizations of vertical mixing, such as those in Munk and Anderson, 1948, would give enhanced mixing for $Ri < 1$ as in turbulent flows mixing persists even when $0.25 < Ri < 1.0$. Hence, our shear and Richardson-number diagnostics can be interpreted as qualitative indicators of changes in mixing potential. The wind-only experiment exhibits a robust increase in near-surface shear and a systematic reduction in daily Ri during tip jet events, consistent with the concurrent MLD deepening and surface-salinity increase; this supports our proposed mechanism, while higher-frequency output would be required to quantify turbulence more directly.

Computational costs also restricted us to five ensemble members of six years each per forcing scenario, which limits our ability to assess large-scale impacts on slower or remote processes such as the AMOC. However, the ensemble members show consistent responses in the key diagnostics used in this study (MLD, buoyancy content, and salinity), increasing confidence in the inferred mechanisms. The limited ensemble size and duration primarily reduce our ability to resolve interannual variability and to compare individual years within the six-year integrations (e.g., year 1 versus year 5) in a statistically robust way.

Another limitation concerns the idealized nature of the applied forcing. Our experiments isolate the ocean response to a westerly Greenland tip jet forcing pattern, rather than to the full spectrum of high-frequency atmospheric forcing around southern Greenland. The wind-stress and heat-flux anomalies were derived from composite westerly tip jet events, averaged over all identified occurrences from 1969 to 2022, and combined with the highest observed westerly tip jet frequency on record (2014–2015). Because the control simulation is forced with a repeated climatological annual cycle, the experimental design cannot fully separate the effect of the specific spatial structure of westerly tip jets from the more general effect of episodic high-frequency wind and heat-flux variability. Therefore, part of the response identified here may be representative of intense winter atmospheric forcing more broadly. At the same time, the imposed anomalies retain the characteristic spatial structure of westerly tip jets, including localized forcing over the central Irminger Sea, where these events produce the strongest negative buoyancy flux anomalies. Our results should therefore be interpreted as the response to strong canonical westerly tip jet forcing and, not as a complete representation of all Greenland mesoscale wind events. A more realistic distribution of westerly, easterly, and other tip jet-like events could alter both the magnitude of the mixed-layer response and the relative importance of heat loss and wind stress. In addition, tip jet properties may evolve as air–sea temperature gradients weaken, potentially altering their intensity, frequency, and spatial structure. Despite these uncertainties, our configuration provides a controlled framework to disentangle and compare the dynamical impacts of wind stress and heat loss associated with canonical westerly tip jet events on Irminger Sea convection.

The role of wind stress in controlling convection intensity is particularly relevant under climate change. Deep-convection regions are already experiencing steady surface warming, and recent shifts in the Mediterranean already demonstrate how reduced air–sea temperature differences weaken heat loss and convection (Josey and Schroeder, 2023; Parras-Berrocal et al., 2022; Somot et al., 2006). A similar reduction in thermal forcing is projected for the Subpolar Gyre (Josey et al., 2019; Koenigk et al., 2021; Oltmanns et al., 2018), whereas wind stress forcing there is not expected to exhibit a comparable downward trend this century (Fedorov et al., 2025). In our experiments, wind stress -driven salinity anomalies enhance convection, but their effect is weaker and less persistent than that of surface heat loss. Therefore, while wind stress is unlikely to fully compensate

for reduced thermal forcing under future warming, it may still delay or modulate the decline of convection. At the same time, enhanced Greenland meltwater input is expected to increase upper ocean stratification and shoal deep convection in the subpolar gyre (Schiller-Weiss et al., 2024) potentially increasing the relative importance of wind stress -driven triggering. The robustness of this mechanism in coupled climate models remains uncertain, as atmospheric feedbacks could alter both the frequency and intensity of tip jets (Bakalian et al., 2007; Moore, 2012; Moore and Renfrew, 2005). Nevertheless, our ocean-only, prescribed-forcing experiments likely overestimate the persistence of the wind stress effect by neglecting atmospheric feedbacks; we therefore interpret them as a qualitative upper bound on the influence of wind stress in sustaining convection under reduced thermal forcing.

Data Availability. Data were processed in MATLAB R2022b/R2023a. Data and scripts required to reproduce the figures are provided via a view-only OSF link [https://osf.io/bj9wn/overview?view_only=a34f660543f1427cad3ed0299ec3b5aa] in 'Tip_Jets_convection.zip'. The anomalies used in the POP forcing are provided via the same view-only OSF link [https://osf.io/bj9wn/overview?view_only=a34f660543f1427cad3ed0299ec3b5aa] in 'POP_Tip_Jet_SHF_TAUXY_crrctd.nc'. Full modelled datasets are not publicly available due to large data sizes.

Author contributions

A. M. Fedorov: Data curation, Formal Analysis, Visualisation, Validation, Methodology, Investigation, Writing (original draft preparation), Writing (review and editing)
M.F. de Jong: Conceptualization, Funding acquisition, Project administration, Supervision, Writing (review and editing)
C.E. Wieners: Conceptualization, Funding acquisition, Methodology, Supervision, Writing (review and editing)
E. Duyck: Methodology, Supervision, Writing (review and editing)
H.A. Dijkstra: Conceptualization, Writing (review and editing)

Competing interests

There are no competing interests to declare.

Acknowledgement

The model simulations and the analysis of all model output were conducted on the Dutch National Supercomputer Snellius within the NWO–SURF project 2023.006 (PI: Wieners). The authors acknowledge Michael Kliphuis (IMAU, Utrecht University) for carrying out the POP simulations and for his technical support. This research was funded by the UU–NIOZ project "The impact of atmospheric noise on the Atlantic meridional overturning circulation."

Literature

Bakalian, F., Hameed, S., and Pickart, R.: Influence of the Icelandic Low latitude on the frequency of Greenland tip jet events: Implications for Irminger Sea convection, J. Geophys. Res., 112, C04020, https://doi.org/10.1029/2006JC003807, 2007.

Biló, T. C., Straneo, F., Holte, J., and Le Bras, I. A. -A.: Arrival of New Great Salinity Anomaly Weakens Convection in the Irminger Sea, Geophys. Res. Lett., 49, e2022GL098857, https://doi.org/10.1029/2022GL098857, 2022.

Coquereau, A., Foukal, N. P., and Våge, K.: Extreme wind events responsible for an outsized role in shelf-basin exchange around the southern tip of Greenland, Sci. Adv., 10, https://doi.org/10.1126/sciadv.adp9266, 2024.

Desbruyères, D. G., Mercier, H., Maze, G., and Daniault, N.: Surface predictor of overturning circulation and heat content change in the subpolar North Atlantic, Ocean Science, 15, 809–817, https://doi.org/10.5194/os-15-809-2019, 2019.

Doyle, J. D. and Shapiro, M. A.: Flow response to large-scale topography: the Greenland tip jet, Tellus A: Dynamic Meteorology and Oceanography, 51, 728, https://doi.org/10.3402/tellusa.v51i5.14471, 1999.

DuVivier, A. K. and Cassano, J. J.: Evaluation of WRF Model Resolution on Simulated Mesoscale Winds and Surface Fluxes near Greenland, Mon. Weather Rev., 141, 941–963, https://doi.org/10.1175/MWR-D-12-00091.1, 2013.

DuVivier, A. K., Cassano, J. J., Craig, A., Hamman, J., Maslowski, W., Nijssen, B., Osinski, R., and Roberts, A.: Winter Atmospheric Buoyancy Forcing and Oceanic Response during Strong Wind Events around Southeastern Greenland in the Regional Arctic System Model (RASM) for 1990–2010*, J. Clim., 29, 975–994, https://doi.org/10.1175/JCLI-D-15-0592.1, 2016.

Duyck, E. and De Jong, M. F.: Circulation Over the South-East Greenland Shelf and Potential for Liquid Freshwater Export: A Drifter Study, Geophys. Res. Lett., 48, e2020GL091948, https://doi.org/10.1029/2020GL091948, 2021.

Duyck, E., Gelderloos, R., and de Jong, M. F.: Wind-Driven Freshwater Export at Cape Farewell, J. Geophys. Res. Oceans, 127, e2021JC018309, https://doi.org/10.1029/2021JC018309, 2022.

Fedorov, A. M. and Bashmachnikov, I. L.: Accuracy of the deep convection intensity from a limited number of casts, Dynamics of Atmospheres and Oceans, 92, 101164, https://doi.org/10.1016/j.dynatmoce.2020.101164, 2020.

Fedorov, A. M., Bashmachnikov, I. L., Iakovleva, D. A., Kuznetsova, D. A., and Raj, R. P.: Deep convection in the Subpolar Gyre: Do we have enough data to estimate its intensity?, Dynamics of Atmospheres and Oceans, 101, 101338, https://doi.org/10.1016/j.dynatmoce.2022.101338, 2023.

Fedorov, A. M., Wieners, C. E., de Jong, M. F., and Dijkstra, H. A.: Understanding the Greenland Tip Jet Role in the Future: Declining Surface Heat Loss in a High-Resolution CESM Simulation (2015–99), J. Clim., 38, 4209–4221, https://doi.org/10.1175/JCLI-D-24-0187.1, 2025.

Fu, Y., Lozier, M. S., Biló, T. C., Bower, A. S., Cunningham, S. A., Cyr, F., de Jong, M. F., deYoung, B., Drysdale, L., Fraser, N., Fried, N., Furey, H. H., Han, G., Handmann, P., Holliday, N. P., Holte, J., Inall, M. E., Johns, W. E., Jones, S., Karstensen, J., Li, F., Pacini, A., Pickart, R. S., Rayner, D., Straneo, F., and Yashayaev, I.: Seasonality of the Meridional Overturning Circulation in the subpolar North Atlantic, Commun. Earth Environ., 4, 181, https://doi.org/10.1038/s43247-023-00848-9, 2023.

Gill, A. E.: Atmosphere-Ocean Dynamics, Academic Press, San Diego, 356–359 pp., 1982.

Good, P.: Permutation, Parametric and Bootstrap Tests of Hypotheses, Springer-Verlag, New York, https://doi.org/10.1007/b138696, 2005.

Grist, J. P., Josey, S. A., and Sinha, B.: Observed and Projected Changes in North Atlantic Seasonal Temperature Reduction and Their Drivers, J. Geophys. Res. Oceans, 128, e2023JC019837, https://doi.org/10.1029/2023JC019837, 2023.

Howard, L. N.: Note on a paper of John W. Miles, J. Fluid Mech., 10, 509–512, https://doi.org/10.1017/S0022112061000317, 1961.

Jackson, L. C., Kahana, R., Graham, T., Ringer, M. A., Woollings, T., Mecking, J. V., and Wood, R. A.: Global and European climate impacts of a slowdown of the AMOC in a high resolution GCM, Clim. Dyn., 45, 3299–3316, https://doi.org/10.1007/s00382-015-2540-2, 2015.

de Jong, M. F. and de Steur, L.: Strong winter cooling over the Irminger Sea in winter 2014-2015, exceptional deep convection, and the emergence of anomalously low SST, Geophys. Res. Lett., 43, 7106–7113, https://doi.org/10.1002/2016GL069596, 2016.

de Jong, M. F., Oltmanns, M., Karstensen, J., and de Steur, L.: Deep Convection in the Irminger Sea Observed with a Dense Mooring Array, Oceanography, 31, 50–59, https://doi.org/10.5670/oceanog.2018.109, 2018.

de Jong, M. F., Fogaren, K. E., Le Bras, I., McRaven, L., and Palevsky, H. I.: Atmospheric Forcing Dominates the Interannual Variability of Convection Strength in the Irminger Sea, J. Geophys. Res. Oceans, 130, e2023JC020799, https://doi.org/10.1029/2023JC020799, 2025.

Josey, S. A. and Schroeder, K.: Declining winter heat loss threatens continuing ocean convection at a Mediterranean dense water formation site, Environmental Research Letters, 18, 024005, https://doi.org/10.1088/1748-9326/aca9e4, 2023.

Josey, S. A., Jong, M. F., Oltmanns, M., Moore, G. K., and Weller, R. A.: Extreme Variability in Irminger Sea Winter Heat Loss Revealed by Ocean Observatories Initiative Mooring and the ERA5 Reanalysis, Geophys. Res. Lett., 46, 293–302, https://doi.org/10.1029/2018GL080956, 2019.

Koenigk, T., Fuentes-Franco, R., Meccia, V. L., Gutjahr, O., Jackson, L. C., New, A. L., Ortega, P., Roberts, C. D., Roberts, M. J., Arsouze, T., Iovino, D., Moine, M.-P., and Sein, D. V.: Deep mixed ocean volume in the Labrador Sea in HighResMIP models, Clim. Dyn., 57, 1895–1918, https://doi.org/10.1007/s00382-021-05785-x, 2021.

Large, W. G. and Crawford, G. B.: Observations and Simulations of Upper-Ocean Response to Wind Events during the Ocean Storms Experiment, J. Phys. Oceanogr., 25, 2831–2852, https://doi.org/10.1175/1520-0485(1995)025<2831:OASOUO>2.0.CO;2, 1995.

Large, W. G. and Yeager, S. G.: Diurnal to Decadal Global Forcing for Ocean and Sea-Ice Models: The Data Sets and Flux Climatologies, NCAR Technical Note, National Center for Atmospheric Research, Boulder, Colorado, 111 pp., 2004.

Large, W. G., McWilliams, J. C., and Doney, S. C.: Oceanic vertical mixing: A review and a model with a nonlocal boundary layer parameterization, Reviews of Geophysics, 32, 363–403, https://doi.org/10.1029/94RG01872, 1994.

Li, F., Lozier, M. S., Bacon, S., Bower, A. S., Cunningham, S. A., de Jong, M. F., deYoung, B., Fraser, N., Fried, N., Han, G., Holliday, N. P., Holte, J., Houpert, L., Inall, M. E., Johns, W. E., Jones, S., Johnson, C., Karstensen, J., Le Bras, I. A., Lherminier, P., Lin, X., Mercier, H., Oltmanns, M., Pacini, A., Petit, T., Pickart, R. S., Rayner, D., Straneo, F., Thierry, V., Visbeck, M., Yashayaev, I., and Zhou, C.: Subpolar North Atlantic western boundary density anomalies and the Meridional Overturning Circulation, Nat. Commun., 12, 3002, https://doi.org/10.1038/s41467-021-23350-2, 2021.

Lozier, M. S., Li, F., Bacon, S., Bahr, F., Bower, A. S., Cunningham, S. A., de Jong, M. F., de Steur, L., deYoung, B., Fischer, J., Gary, S. F., Greenan, B. J. W., Holliday, N. P., Houk, A., Houpert, L., Inall, M. E., Johns, W. E., Johnson, H. L., Johnson, C., Karstensen, J., Koman, G., Le Bras, I. A., Lin, X., Mackay, N., Marshall, D. P., Mercier, H., Oltmanns, M., Pickart, R. S., Ramsey, A. L., Rayner, D., Straneo, F., Thierry, V., Torres, D. J., Williams, R. G., Wilson, C., Yang, J., Yashayaev, I., and Zhao, J.: A sea change in our view of overturning in the subpolar North Atlantic, Science (1979)., 363, 516–521, https://doi.org/10.1126/science.aau6592, 2019.

Martin, R. and Moore, G. W. K.: Air-sea interaction associated with a Greenland reverse tip jet, Geophys. Res. Lett., 34, L24802, https://doi.org/10.1029/2007GL031093, 2007.

McDougall, T. J. and Barker, P. M.: Getting Started with TEOS-10 and the Gibbs Seawater (GSW) Oceanographic Toolbox, SCOR/IAPSO Working Group 127, 28 pp., 2011.

Miles, J. W.: On the stability of heterogeneous shear flows, J. Fluid Mech., 10, 496–508, https://doi.org/10.1017/S0022112061000305, 1961.

Monin, A. S. and Obukhov, A. M.: Basic laws of turbulent mixing in the surface layer of the atmosphere, Trudy Geofizicheskogo Instituta, 163–187, 1954.

Moore, G. W. K.: Gale force winds over the Irminger Sea to the east of Cape Farewell, Greenland, Geophys. Res. Lett., 30, n/a-n/a, https://doi.org/10.1029/2003GL018012, 2003.

Moore, G. W. K.: A new look at Greenland flow distortion and its impact on barrier flow, tip jets and coastal oceanography, Geophys. Res. Lett., 39, n/a-n/a, https://doi.org/10.1029/2012GL054017, 2012.

Moore, G. W. K. and Renfrew, I. A.: Tip Jets and Barrier Winds: A QuikSCAT Climatology of High Wind Speed Events around Greenland, J. Clim., 18, 3713–3725, https://doi.org/10.1175/JCLI3455.1, 2005.

Munk, W. H. and Anderson, E. R.: Notes on a theory of the thermocline., J. Mar. Res., 7, 276–295, 1948.

Nansen, F.: The Norwegian North polar expedition, 1893-1896; scientific results, Volume 5., Longmans, Green and co, London, New York, Bombay, 1906.

Oltmanns, M., Karstensen, J., and Fischer, J.: Increased risk of a shutdown of ocean convection posed by warm North Atlantic summers, Nat. Clim. Chang., 8, 300–304, https://doi.org/10.1038/s41558-018-0105-1, 2018.

Outten, S. D., Renfrew, I. A., and Petersen, G. N.: An easterly tip jet off Cape Farewell, Greenland. II: Simulations and dynamics, Quarterly Journal of the Royal Meteorological Society, 135, 1934–1949, https://doi.org/10.1002/qj.531, 2009.

Parras-Berrocal, I. M., Vázquez, R., Cabos, W., Sein, D. V., Álvarez, O., Bruno, M., and Izquierdo, A.: Surface and Intermediate Water Changes Triggering the Future Collapse of Deep Water Formation in the North Western Mediterranean, Geophys. Res. Lett., 49, e2021GL095404, https://doi.org/10.1029/2021GL095404, 2022.

Petit, T., Lozier, M. S., Josey, S. A., and Cunningham, S. A.: Atlantic Deep Water Formation Occurs Primarily in the Iceland Basin and Irminger Sea by Local Buoyancy Forcing, Geophys. Res. Lett., 47, e2020GL091028, https://doi.org/10.1029/2020GL091028, 2020.

Pickart, R. S., Spall, M. A., Ribergaard, M. H., Moore, G. W. K., and Milliff, R. F.: Deep convection in the Irminger Sea forced by the Greenland tip jet, Nature, 424, 152–156, https://doi.org/10.1038/nature01729, 2003a.

Pickart, R. S., Straneo, F., and Moore, G. W. K.: Is Labrador Sea Water formed in the Irminger basin?, Deep Sea Research Part I: Oceanographic Research Papers, 50, 23–52, https://doi.org/10.1016/S0967-0637(02)00134-6, 2003b.

Pollard, R. T., Rhines, P. B., and Thompson, R. O. R. Y.: The deepening of the wind-Mixed layer, Geophysical Fluid Dynamics, 4, 381–404, https://doi.org/10.1080/03091927208236105, 1973.

Price, J. F., Weller, R. A., and Pinkel, R.: Diurnal cycling: Observations and models of the upper ocean response to diurnal heating, cooling, and wind mixing, J. Geophys. Res. Oceans, 91, 8411–8427, https://doi.org/10.1029/JC091iC07p08411, 1986.

Renfrew, I. A., Petersen, G. N., Sproson, D. A. J., Moore, G. W. K., Adiwidjaja, H., Zhang, S., and North, R.: A comparison of aircraft-based surface-layer observations over Denmark Strait and the Irminger Sea with meteorological analyses and QuikSCAT winds, Quarterly Journal of the Royal Meteorological Society, 135, 2046–2066, https://doi.org/10.1002/qj.444, 2009a.

Renfrew, I. A., Outten, S. D., and Moore, G. W. K.: An easterly tip jet off Cape Farewell, Greenland. I: Aircraft observations, Quarterly Journal of the Royal Meteorological Society, 135, 1919–1933, https://doi.org/10.1002/qj.513, 2009b.

Schiller-Weiss, I., Martin, T., and Schwarzkopf, F. U.: Emerging Influence of Enhanced Greenland Melting on Boundary Currents and Deep Convection Regimes in the Labrador and Irminger Seas, Geophys. Res. Lett., 51, e2024GL109022, https://doi.org/10.1029/2024GL109022, 2024.

Schmidt, S. and Send, U.: Origin and Composition of Seasonal Labrador Sea Freshwater, J. Phys. Oceanogr., 37, 1445–1454, https://doi.org/10.1175/JPO3065.1, 2007.

Shkolnik, I. M. and Efimov, S. V: Cyclonic activity in high latitudes as simulated by a regional atmospheric climate model: added value and uncertainties, Environmental Research Letters, 8, 045007, https://doi.org/10.1088/1748-9326/8/4/045007, 2013.

Somot, S., Sevault, F., and Déqué, M.: Transient climate change scenario simulation of the Mediterranean Sea for the twenty-first century using a high-resolution ocean circulation model, Clim. Dyn., 27, 851–879, https://doi.org/10.1007/s00382-006-0167-z, 2006.

Sproson, D. A. J., Renfrew, I. A., and Heywood, K. J.: Atmospheric conditions associated with oceanic convection in the south-east Labrador Sea, Geophys. Res. Lett., 35, https://doi.org/10.1029/2007GL032971, 2008.

595 Sproson, D. A. J., Renfrew, I. A., and Heywood, K. J.: A parameterization of Greenland's tip jets suitable for ocean or coupled climate models, J. Geophys. Res. Oceans, 115, https://doi.org/10.1029/2009JC006002, 2010.

Tilinina, N., Gulev, S. K., and Bromwich, D. H.: New view of Arctic cyclone activity from the Arctic system reanalysis, Geophys. Res. Lett., 41, 1766–1772, https://doi.org/10.1002/2013GL058924, 2014.

Våge, K., Pickart, R. S., Moore, G. W. K., and Ribergaard, M. H.: Winter Mixed Layer Development in the Central Irminger
600 Sea: The Effect of Strong, Intermittent Wind Events, J. Phys. Oceanogr., 38, 541–565, https://doi.org/10.1175/2007JPO3678.1, 2008.

Våge, K., Spengler, T., Davies, H. C., and Pickart, R. S.: Multi-event analysis of the westerly Greenland tip jet based upon 45 winters in ERA-40, Quarterly Journal of the Royal Meteorological Society, 135, 1999–2011, https://doi.org/10.1002/qj.488, 2009a.

605 Våge, K., Pickart, R. S., Thierry, V., Reverdin, G., Lee, C. M., Petrie, B., Agnew, T. A., Wong, A., and Ribergaard, M. H.: Surprising return of deep convection to the subpolar North Atlantic Ocean in winter 2007–2008, Nat. Geosci., 2, 67–72, https://doi.org/10.1038/ngeo382, 2009b.

Viebahn, J. P., von der Heydt, A. S., Le Bars, D., and Dijkstra, H. A.: Effects of Drake Passage on a strongly eddying global ocean, Paleoceanography, 31, 564–581, https://doi.org/10.1002/2015PA002888, 2016.

610 van Westen, R. M., Vanderborght, E., Kliphuis, M., and Dijkstra, H. A.: Physics-Based Indicators for the Onset of an AMOC Collapse Under Climate Change, J. Geophys. Res. Oceans, 130, e2025JC022651, https://doi.org/10.1029/2025JC022651, 2025.

Zhou, S., Zhai, X., and Renfrew, I. A.: The Impact of High-Frequency Weather Systems on SST and Surface Mixed Layer in the Central Arabian Sea, J. Geophys. Res. Oceans, 123, 1091–1104, https://doi.org/10.1002/2017JC013609, 2018.

615

Appendix:

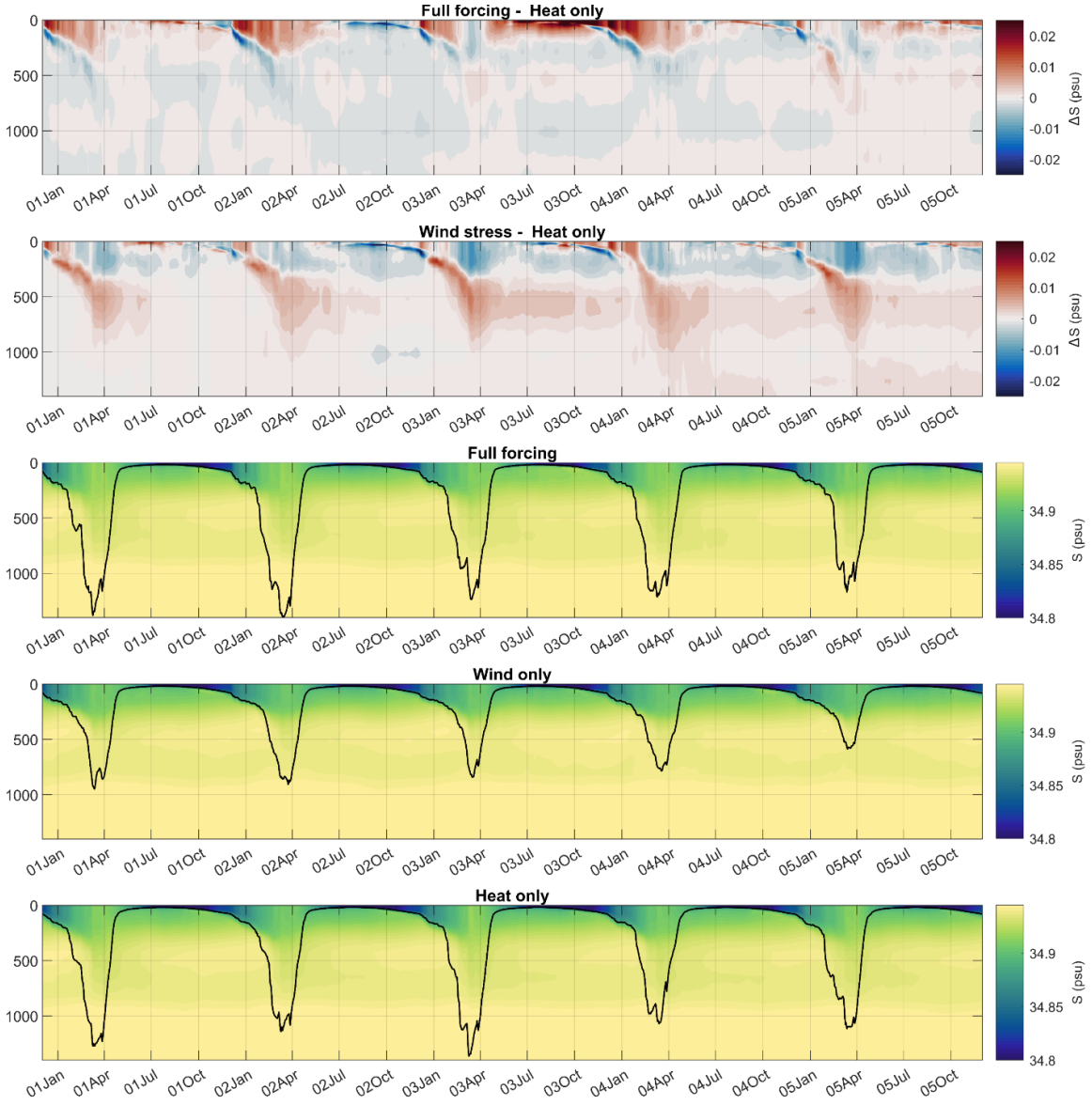

Figure A1. Ensemble-mean salinity and salinity anomalies. Panels from top to bottom show: salinity difference (full-forcing − heat-only), salinity difference (wind-only − heat-only), absolute salinity in the full-forcing run, absolute salinity in the wind-only run, and absolute salinity in the heat-only run.